Applied Catalysis B: Environmental 140–141 (2013) 516–522

Contents lists available at SciVerse ScienceDirect

Applied Catalysis B: Environmental

journal homepage: www.elsevier.com/locate/apcatb

Vapour phase H_2O_2 decomposition on Mn based monolithic catalysts synthesized by innovative procedures

L. Micoli[a], G. Bagnasco[a], M. Turco[a,*], M. Trifuoggi[b], A. Russo Sorge[c], E. Fanelli[a], P. Pernice[a], A. Aronne[a]

[a] Dipartimento di Ingegneria Chimica dei Materiali e della Produzione Industriale, Università di Napoli Federico II, P.le V. Tecchio, 80125 Napoli, Italy
[b] Dipartimento di Scienze Chimiche, Università di Napoli Federico II, Napoli, Italy
[c] Dipartimento di Ingegneria Industriale, Università di Napoli Federico II, Napoli, Italy

ARTICLE INFO

Article history:
Received 15 February 2013
Received in revised form 26 April 2013
Accepted 30 April 2013
Available online 8 May 2013

Keywords:
Sol–gel
MnO_x/ZrO_2 catalyst
H_2O_2 vapour decomposition
Space propulsion

ABSTRACT

Manganese oxide catalysts supported on monolithic yttria stabilized zirconia honeycombs were studied for H_2O_2 decomposition in view of space propulsion applications. The materials were prepared by impregnation (IM), precipitation (PR) and sol–gel (SG) methods and characterized by N_2 adsorption, SEM and H_2 temperature programmed reduction (TPR). The catalytic activity for H_2O_2 decomposition was studied under vapour phase conditions. The tests were carried out in a flow apparatus at $T = 200\,^{\circ}C$, gas hourly space velocity (GHSV) = 2.00 and 2.67 s^{-1}, H_2O_2 concentrations of 11.3 mol%. The redox properties of the catalysts were markedly influenced by the preparation method. In the SG catalyst, a large fraction of Mn was not reducible in the TPR tests differently from the PR and IM materials. Despite this effect, the SG catalyst showed an activity comparable or higher than that of PR and IM, due to a more effective dispersion of Mn species. A too strong effect of space velocity on H_2O_2 conversion was attributed to an autocatalytic effect. A radical mechanism was hypothesized: it was assumed that a reaction between O_2 and Mn species produced radicals that promoted the overall reaction.

1. Introduction

The use of H_2O_2 as propellant for space applications is of great interest due to the lower toxicity and environmental impact of this compound compared with conventional propellants such as those based on hydrazine [1–3]. The reaction of H_2O_2 decomposition is highly exothermic and, under adiabatic conditions can give rise to hot gaseous products (H_2O and O_2) at temperatures ranging from 632 to 953 °C depending on the H_2O_2 concentration (85–98%). These gaseous products can be directly sent to a nozzle to produce the thrust (mono-propellant configuration) or used to burn a fuel, thus releasing further heat and producing a stronger thrust (bi-propellant configuration).

Several materials are active for H_2O_2 decomposition, but those suitable for propulsive applications must fulfil very strict requirements, the most important of which concerns the ability of the catalyst to work in a wide temperature range and the high resistance to thermal and mechanical shocks. Moreover the resistance to poisoning by stabilizing additives that are present in H_2O_2 solutions is required [4].

Several catalysts based on metal oxides were proposed for H_2O_2 propulsive applications [3–8], among these Mn oxides supported on TiO_2 or ZrO_2 appeared very interesting [3,9]. High activity was found with MnO_x/ZrO_2 systems prepared by sol–gel [10]. Catalytic activity was generally studied under liquid phase conditions, whilst, apart from some paper dating back to the sixties [11], catalysts designed for propulsive applications were not tested under vapour phase conditions. Such conditions are relevant for propulsive applications since the catalytic reactor must operate in large part with vaporized H_2O_2.

In view of propulsive applications it is believed that monolithic catalysts are more suitable in comparison with other shapes such as pellets, because they give the advantages of low pressure drop, good distribution of the reactant and high mechanical resistance [12,13]. Different monolithic substrates can be used, such as cordierite that is widely employed for pollutants emission control [14]. In the present work honeycombs made of yttria stabilized zirconia were employed considering the promising results obtained with MnO_x/ZrO_2 powdered catalysts [9,10]. The dispersion of the active phase on the monolithic substrate is a key step for the preparation of the structured catalysts, and is generally performed by a complex procedure comprising a washcoating of the substrate with a suitable oxide (generally alumina) on which the active phase is supported. In the present work Mn based monoliths were prepared by innovative procedures. The traditional methods of impregnation

* Corresponding author. Tel.: +39 0817682259; fax: +39 0815936936.
E-mail address: turco@unina.it (M. Turco).

0926-3373/$ – see front matter © 2013 Elsevier B.V. All rights reserved.
http://dx.doi.org/10.1016/j.apcatb.2013.04.072

and precipitation were properly modified to obtain the dispersion of the active phase on the substrate avoiding the preliminary washcoating. An innovative sol–gel procedure was set aimed at the formation of an uniform layer of active phase on the inner surface of the honeycomb channels exploiting a gelation mechanism likewise to that occurring in the preparation of film by dip-coating. This sol–gel method allows coating of zirconia honeycomb support with a porous layer of zirconia in which the active phase MnO_x is dispersed. All the prepared catalysts were characterized by N_2 adsorption, SEM and H_2 temperature programmed reduction (TPR) techniques. The catalytic activity for vapour phase H_2O_2 decomposition was studied in a laboratory flow plant properly designed.

2. Experimental

2.1. Catalyst preparation

Honeycomb cylindrical ZrO_2 supports stabilized with 8 mol% Y_2O_3 (l = 3.0 cm, d = 1.3 cm, square channel density = 62 cm^{-2}) were supplied by Céramiques Techniques Industrielles Company (Salindres, France). The active phase was dispersed on the supports by three methods: a layer of manganese–yttrium–zirconium mixed-oxide nanocomposite by sol–gel (a), MnO_x by precipitation (b) and impregnation (c).

2.1.1. Sol–gel

The preparation of catalysts has required proper changes with respect to the sol–gel route previously set [10]. In fact, in this case the goal of the synthesis procedure is to realize a suitable stock solution in which to dip the honeycombs. The stock solution was obtained by diluting with a proper amount of 1-propanol the solution of precursors that correspond to a nominal Mn content of 30 wt% (with respect to the matrix, whose molar composition is $95ZrO_2{\cdot}5Y_2O_3$). This is an alcoholic (1-propanol) solution formed by zirconium(IV) propoxide, acetylacetone (Hacac), with a molar ratio Zr: Hacac = 1: 0.5, and the proper amount of yttrium(III) chloride hexahydrate and manganese(II) nitrate pentahydrate ($Zr{:}YCl_3{\cdot}6H_2O{:}Mn(NO_3)_2{\cdot}5H_2O$ = 1:0.105:0.738) [10]. The resulting solution was hydrolyzed at room temperature for 2 weeks before the honeycombs covering.

The honeycombs were coated at room temperature by dipping them into the stock solution so that the internal surface of the square channels was fully covered by a layer of precursors solution. After that they were withdrawn from the stock solution, dried at 110 °C and then annealed in air at 550 °C for 16 h.

The actual Mn content deposited on the honeycombs surface with this procedure was evaluated by inductively coupled plasma associated with a mass spectrometry detector (ICP-MS). Different measurements were performed both on the outer (shell) and inner (core) surface of honeycombs according to the following procedure. The core was separated from the shell and both parts were ground to fine powder, then 0.2 g of each were digested in 5 mL of HNO_3 and H_2O_2 solution. The Mn containing solutions were analyzed using an ICP-MS Bruker Aurora m90, quartz nebulizer, glass spray chamber, quartz monobloc torch and auto sampler SPS3. The concentration of manganese in the solution, was reported in mg of manganese per gram of catalyst, giving 5.3 mg/g in the shell and 4.4 mg/g in the core, and an average content of 4.8 mg/g (0.48 wt%).

2.1.2. Precipitation

The honeycomb support was introduced into a 100 mL of 0.65 mol L^{-1} aqueous $Mn(II)(C_2H_3O_2)_2$ solution under stirring at 50 °C. Then 2 mL of concentrated NH_4OH was added to precipitate $Mn(OH)_2$ on the support surface. This precipitation step lasts about 1 h. Afterwards the material was drained and oven dried at 120 °C for 2 h. Finally the sample was calcined at 500 °C with 6 L h^{-1} air flow, to transform $Mn(OH)_2$ in Mn_2O_3 [15]. This procedure was repeated five times to get the desired manganese content. From the weight increase of the support, an actual Mn content of 0.65 wt% was estimated, assuming a complete transformation into Mn_2O_3.

2.1.3. Impregnation

The impregnation was carried out under vacuum to help the solution penetration into the honeycomb porosity and to obtain a more uniform dispersion. After evacuation in a flask of 100 mL, an aqueous 0.65 mol L^{-1} $Mn(II)(C_2H_3O_2)_2$ solution, at T = 40 °C, was dripped up to complete wetting of the support, with no excess solution. Afterwards the impregnated support was dried at 120 °C for 2 h and then heated at 500 °C in air flow (6 L h^{-1}) for 2 h to get manganese acetate decomposition and Mn_2O_3 formation [16]. This procedure was repeated three times to achieve the desired active phase content. From the weight increase of the support, the actual Mn content was estimated to be 1.43 wt%, assuming a full transformation into Mn_2O_3.

Energy-dispersive spectroscopy (EDS) analysis carried out on different sections of the monoliths prepared by precipitation and impregnation showed a uniform dispersion of the active phase along the channels of the substrate.

2.2. Catalyst characterization

EDS and SEM measurements were carried out in a Philips XL30 apparatus. SEM micrographs were obtained out on small bits taken from different points of the monoliths that were ground to powder.

Surface areas were measured by N_2 adsorption at −196 °C using a Micromeritics ASAP 2020 apparatus. This apparatus, equipped with a special sample cell with accurate thermal stabilization, allowed to carry out N_2 adsorption tests on the entire honeycomb catalyst and to achieve an accuracy of ±0.02 m^2 g^{-1} in surface area values.

TPR tests were carried out on the monolithic catalysts, using a laboratory apparatus [17], with a 2% H_2/Ar mixture (Q = 150 cm^3 min^{-1}) and heating rate of 10 °C min^{-1} up to 800 °C. The entire monolithic sample was loaded in a quartz down-flow cell, with an enlarged central zone (i.d. = 1.9 cm, l = 6 cm).

2.3. Catalytic activity measurements

H_2O_2 decomposition tests in the vapour phase were carried out in an experimental apparatus operating in flow at atmospheric pressure (Fig. 1).

The reactor was a glass tube (i.d. = 0.6 cm, l = 40 cm) with a central enlarged section (i.d. = 1.9 cm, l = 8 cm) in which the cylindrical honeycomb catalyst was precisely accommodated. The tube sizing after the catalyst was reduced to 0.2 cm to limit the contribution of the homogeneous reaction. The reaction temperature was measured by a K thermocouple sited close to the catalyst. The reactor was properly designed to allow the vaporization and preheating of the feed mixture. A concentrated H_2O_2/H_2O solution supplied by Evonik Degussa (87.5 wt% H_2O_2, $NaNO_3$ < 20 mg L^{-1}, Sn < 9 mg L^{-1}, P < 0.2 mg L^{-1}) was diluted to 50 wt% H_2O_2 and was fed to the reactor by an Alltech HPLC 301 metering pump. Higher concentration of H_2O_2 could not be treated in the pump due to safety problems. Chromatographic He (99.995%) was added as carrier and was fed by a Brooks MFC regulator. The products coming out from the reactor flowed through an ice trap and an anhydrous KOH trap for the separation of H_2O and not converted H_2O_2, then they were sent to a thermal conductivity detector (TCD) for the continuous analysis of O_2. The concentration of O_2 measured by the TCD allowed to calculate the O_2 flow rate, that directly gave the rate of H_2O_2 decomposition. In this way the rate of H_2O_2 decomposition was measured continuously as a function of time. The reactant feed was

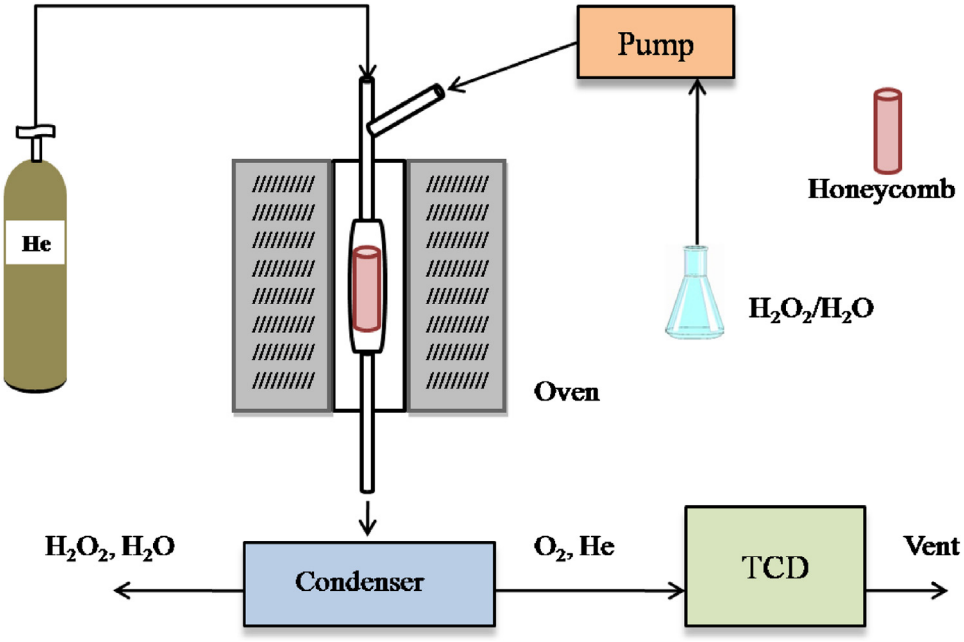

Fig. 1. Apparatus for H_2O_2 decomposition tests.

maintained until the attainment of constant product composition, and in all cases for at least 30 min.

Catalytic tests were carried out at $T = 200\,^{\circ}C$, with total feed flow rates ($H_2O_2 + H_2O + He$) of 223 (low rate) or 280 (high rate) mL min^{-1} and constant feed composition. These flow rates correspond to gas hourly space velocities (GHSV) = 2.00 and 2.67 s^{-1} respectively. Molar feed rates and the feed composition are reported in Table 1. Blank tests with the reactor filled with inert α-Al_2O_3 (same void space as the monolithic catalysts) showed that the homogeneous H_2O_2 decomposition was negligible under these conditions.

3. Results and discussion

3.1. Sol–gel synthesis of the catalysts

The covering procedure of honeycombs is based on the possibility to realize a uniform layer of gel on their surface exploiting a gelation mechanism likewise to that occurring in the preparation of films by dip-coating. Therefore, it is expected that gelation is mainly driven by solvent evaporation. Moreover, it is essential to satisfy the chemical affinity requirements between the precursors solution and the support. For this reason the chemical composition of the honeycombs was chosen to assure the greatest affinity with the stock solution.

The starting solution contains several compounds and ionic species, such as $Zr(OPr)_4$, Y^{3+}, Mn^{2+}, that exhibit both a very high reactivity towards hydrolysis and good ability to form several complexes with oxygen donor ligands, among them water, alcohols and β-diketones. The selected Zr:Hacac molar ratio (1:0.5) allowed to control simultaneously the reactivity of all these species giving a stable solution formed by partially hydrolyzed oligomers, $Zr(OPr)_x(OH)_y$ avoiding the precipitation of hydrated zirconium oxide–alkoxide aggregates. The stability towards the gelation was controlled by a suitable dilution degree. After dipping the wet honeycomb was dried slowly at 110 °C giving the evaporation of solvents and, simultaneously, the formation of a uniform layer of gel on the honeycomb surface.

According to [10], an annealing of 16 h at 500 °C was required to transform the gel layer into a stable porous layer of catalyst as shown in Fig. 2, where the SEM microphotographs, at two different magnification, of the honeycomb inner surface subjected to covering procedure is displayed. From these images the uniformity of the catalyst layer covering the inner surface of the honeycomb is seen.

3.2. Textural and redox properties

The N_2 adsorption isotherms of all samples are reported in Fig. 3. The desorption curves are fully overlapped with the adsorption ones, suggesting that hysteresis phenomena are absent. The isotherms are of type II according to the IUPAC classification [18] and are typical of solids with little or no pore volume. Surface areas calculated from these data are reported in Table 2. Surface area increases slightly with the introduction of the active phase onto the support. As the content of active phase is always much higher than that corresponding to monolayer coverage (0.21% Mn, assuming the presence of quasi-cubic Mn_2O_3 with unit cell size $a = 0.941$ nm [19]), it can be supposed that the support is completely covered

Table 1
Feed flow rates and composition for tests of catalytic H_2O_2 decomposition.

Substance	Feed flow rate (mmol min^{-1})		Feed composition (mol%)
	GHSV = 2.00 s^{-1}	GHSV = 2.67 s^{-1}	
H_2O_2	0.65	0.82	11.3
H_2O	1.23	1.54	21.4
He	3.86	4.85	67.3

Table 2
Surface area of the catalysts.

Sample	Preparation method	Surface area	
		$m^2\ g_{cat}^{-1}$	$m^2\ g_{Mn}^{-1}$
Support	–	0.45	–
SG	Sol–gel	0.63	131
PR	Precipitation	0.73	112
IM	Impregnation	0.63	44

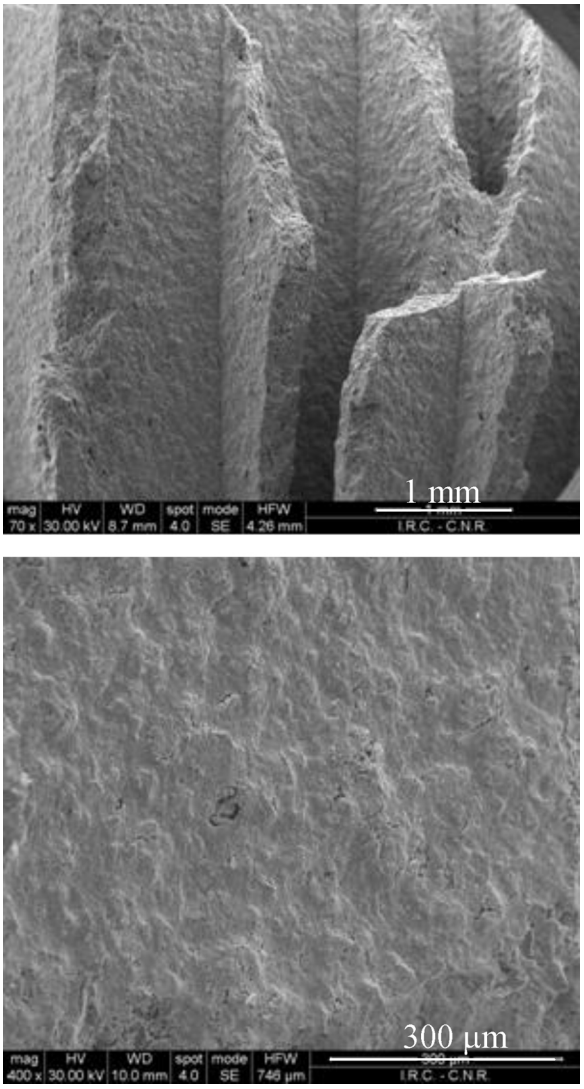

Fig. 2. SEM micrograph of SG catalyst.

and gives no contribution to the surface area of the catalysts. The surface area values referred to the Mn content (fourth column of Table 2) are quite high and confirm the higher dispersion of the active phase in the sample prepared by the sol–gel method.

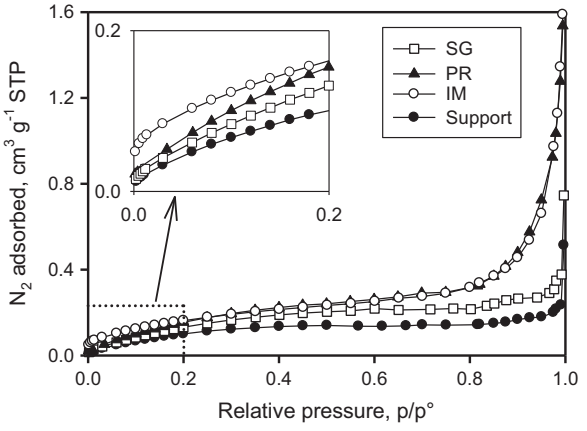

Fig. 3. N_2 adsorption isotherms on SG, PR, IM and the pure support at −196 °C.

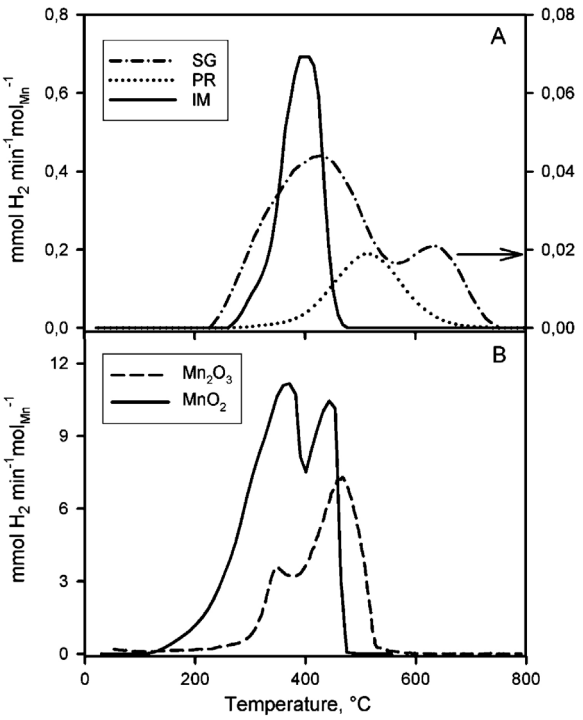

Fig. 4. TPR profiles of: (A) catalysts SG, PR and IM, and (B) reference oxides Mn_2O_3 and MnO_2. Note the different scale used for the SG catalyst.

The redox properties of the catalysts were investigated by TPR measurements. The TPR profiles of the catalysts are collected in Fig. 4 together with the profiles of the reference oxides Mn_2O_3 and MnO_2. The ceramic support gives no TPR signal. The reference oxides Mn_2O_3 and MnO_2 were prepared by decomposition, at 500 °C for 2 h in air flow, of $Mn(C_2H_3O_2)_2$ and $Mn(NO_3)_2{\cdot}5H_2O$ respectively. It must be noted that under the conditions of the thermal treatment the stable Mn oxide is Mn_2O_3 [20], so it is expected that this compound is formed from the decomposition of a Mn salt in air. However the formation of Mn oxides can be also driven by kinetic factors, that is by a possible competition between oxidation and reduction reactions, due to the presence of O_2 and products of the salt decomposition: since the oxide MnO_2 is only slightly less stable than Mn_2O_3 under these conditions (MnO_2 becomes more stable at $T < 400$ °C [20]), it can be obtained when some oxidizing species are present, for example in the decomposition of $Mn(NO_3)_2{\cdot}5H_2O$ [21]. The phases obtained by thermal treatment are not modified when they are quenched to room temperature because the rate of conversion between different Mn oxides is very low at $T < 500$ °C [20].

The TPR profile of Mn_2O_3 shows a main signal with maximum at 460 °C and a smaller one at 345 °C (Fig. 4B). The total amount of H_2 consumed is 0.51 mol_{H_2}/mol_{Mn}, in agreement with the value expected for the reduction $Mn_2O_3 \rightarrow MnO$. The two TPR signals are probably due to a stepwise reduction of Mn_2O_3 [22]:

$$Mn_2O_3 \rightarrow Mn_3O_4 \rightarrow MnO \quad (1)$$

The profile of MnO_2 shows two peaks at temperatures (360 and 450 °C) close to those observed for Mn_2O_3, but in this case the reduction begins at much lower temperature and the two peaks have comparable intensities (Fig. 4B). The total amount of H_2 consumed is 0.92 mol_{H_2}/mol_{Mn}, that is close to the amount expected for the reduction $MnO_2 \rightarrow MnO$. The asymmetric shape of the low temperature peak suggests that it is formed by two

Table 3
TPR measurements on the catalysts.

Sample	TPR peak (°C)	H_2 consumed (μmol g^{-1})	Mn content (μmol g^{-1})
SG	425, 629	9.8	87
PR	514	49	118
IM	400	171	260

overlapping signals. These results can be explained assuming that the reduction of MnO_2 occurs in three steps, that is:

$$MnO_2 \rightarrow Mn_2O_3 \rightarrow Mn_3O_4 \rightarrow MnO \quad (2)$$

The first two steps occur at very close temperatures, giving rise to the asymmetric TPR peak. This step reduction of MnO_2 agrees with literature data [3,22].

The above results confirm that under the conditions of the TPR tests, manganese oxides are reduced to MnO, as previously suggested [3]. Moreover these data show that the oxides MnO_2 and Mn_2O_3 are not easily distinguished by the position of the TPR peaks, because their signals appear at very close temperatures: a distinction can be only made on the base of the relative intensity of the TPR signals and considering that the reduction of MnO_2 begins at lower temperature.

The TPR profiles of the catalysts (Fig. 4A) appear quite different from those of the reference Mn oxides and from each other, indicating that the redox properties of the MnO_x phases are influenced by the interaction with the support and by the preparation method. The amounts of H_2 consumed, calculated from the areas of the TPR peaks and are reported in Table 3.

The profile of SG shows two signals: the first is very broad and covers the range of temperatures typical of MnO_2 and Mn_2O_3, while the second appears at much higher temperature. The broad low temperature signal can be related to the presence of Mn species in two oxidation states, (III) and (IV); the high temperature signal indicates hardly reducible Mn species. It is worth noting the low intensity of these signals: as shown in Table 3, the amount of H_2 consumed is small compared to the Mn content, indicating that only a limited amount of Mn is reduced. A possible explanation is that Mn species, being intimately mixed with zirconia in the catalytic film, can give rise to a stable mixed oxide and for this reason are not reducible under the present conditions. In fact, it is known that Mn can be incorporated (mainly as Mn^{2+} ion) into the zirconia lattice [23].

The TPR profile of PR shows a symmetric peak at a temperature slightly higher than that of pure Mn_2O_3. On the base of the above thermodynamic considerations, the thermal treatment applied to the catalyst should favour the formation of Mn_2O_3. The amount of H_2 consumed (Table 3) is lower than that corresponding to the reduction $Mn_2O_3 \rightarrow MnO$: if a Mn(II) state is assumed after the reduction, the average oxidation state of Mn before the reduction would be 2.6 instead of the expected 3.0. In this case, differently from the SG catalyst, the low H_2 consumption cannot be related to the formation of a stable mixed oxide, because Mn oxide is not intimately mixed with zirconia. Instead, it must be related specifically to the preparation method: it can be supposed that during the thermal treatment, the oxidizing action of O_2 is counteracted by the reducing action of organic compounds, for example acetate ions that remained adsorbed on the precipitate of Mn hydroxide. The value of Mn oxidation state 2.6 suggests the presence of the mixed valence oxide Mn_3O_4 (Mn ox. state = 2.67): this would also explain the presence of one TPR signal, because the reduction would occur in one instead of two steps, according to Eq. (1).

The TPR curve of the IM catalyst shows a large signal at 400 °C with an asymmetry that suggests some contribution by a lower temperature signal. The peak occurs at temperature lower than

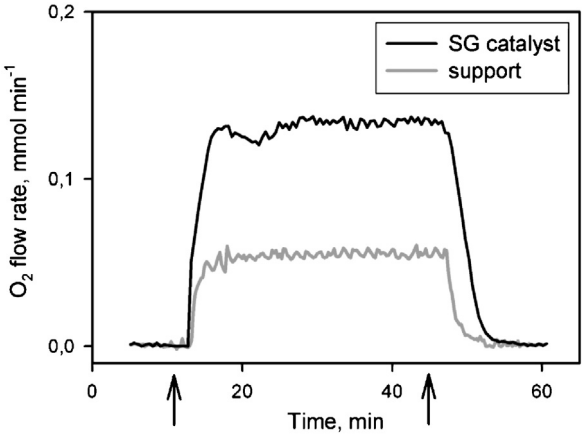

Fig. 5. H_2O_2 decomposition tests on the SG catalyst and the pure support: O_2 flow rate as a function of time. T = 200 °C; feed composition = 11.3% H_2O_2, 21.4% H_2O, He balance; GHSV = 2.67 s^{-1}. The arrows on the time axis indicate the beginning and the end of the H_2O_2 feed.

that of Mn_2O_3, indicating a higher reducibility compared with the pure oxide, probably related to a higher dispersion: however the shifting to lower temperature can be also related to the presence of some MnO_2. This is confirmed by the value of H_2 consumption (Table 3): in fact, assuming that also in this case Mn is reduced to the state Mn(II), the value of H_2 consumption corresponds to an average Mn oxidation state of 3.3 before the TPR test. The higher Mn oxidation state compared with the PR catalyst can be explained by the different preparation method: in the preparation of PR, Mn hydroxide was precipitated at 40 °C and could adsorb appreciable amounts of acetate ions, while in the case of IM, the decomposition of $Mn(C_2H_3O_2)_2$ occurred at higher temperature, so it is likely that most acetate ions were eliminated before the formation of a Mn oxide/hydroxide phase, and the amount of organic residues adsorbed was more limited. So the reducing effect of organic compounds was lower in the IM catalyst.

In conclusion, TPR data show that the redox properties of the MnO_x/ZrO_2 catalysts are markedly influenced by the presence of the support and by the preparation method. In the catalyst prepared by sol–gel, a strong interaction of Mn with zirconia makes a large fraction of Mn not reducible under the present conditions, while a similar effect is not observed for the materials prepared by precipitation or impregnation. The Mn(III) oxidation state prevails in both PR and IM catalysts. The catalyst PR appears less reducible than the reference Mn_2O_3 oxide, probably due to the presence of the oxide Mn_3O_4 that needs a higher temperature for reduction. On the other hand, the catalyst IM appears more reducible than the unsupported Mn_2O_3 oxide, due to the presence of some MnO_2: this oxide is probably absent in PR.

3.3. Catalytic activity

The results of tests carried out on the SG catalyst and the pure support with space velocity of 2.67 s^{-1} are reported in Fig. 5 in terms of flow rate of O_2 produced as a function of time. After introduction of the H_2O_2 feed, the O_2 flow rate shows a transitory variation for a few minutes before stationary conditions are achieved. A similar behaviour was observed with all catalysts and stationary conditions were obtained in all cases after less than 15 min. The tests lasting about 30 min were repeated three times on each sample and same results were obtained. From the final constant O_2 flow rates, H_2O_2 conversions were calculated for all catalysts. These data are reported in Fig. 6 for the catalysts SG, PR and IM and the pure support tested at 200 °C, with space velocity of 2.00 and 2.67 s^{-1}.

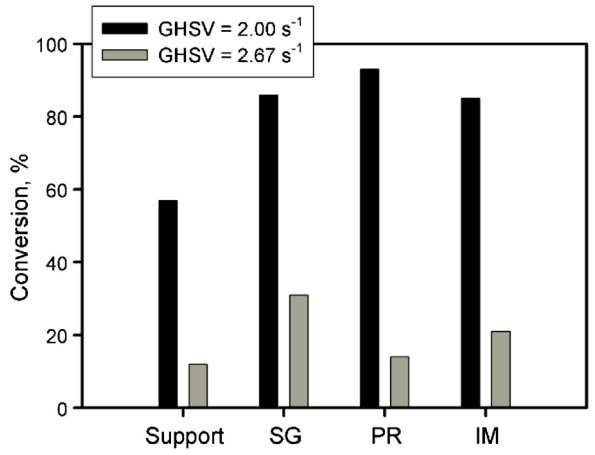

Fig. 6. H_2O_2 conversion on the pure support, SG, PR and IM at $T = 200\,^{\circ}C$; feed composition = 11.3% H_2O_2, 21.4% H_2O, He balance.

Two aspects of these results need a special consideration: (i) H_2O_2 conversion increases strongly with decreasing space velocity, especially for PR and IM catalysts and (ii) the pure support has noticeable activity. The strong increase of H_2O_2 conversion with decreasing space velocity cannot be due to an increase of temperature because the temperature was controlled by a thermocouple located in close proximity of the end of the monolithic catalyst. Instead the results can be explained by an autocatalytic reaction. Little information is available about the mechanism of H_2O_2 decomposition on Mn oxide based catalysts. Some authors suggest that a reaction with electron exchange between H_2O_2 and the catalyst surface creates free radicals that then initiate a chain reaction producing H_2O and O_2 as final products [24,25]. Others, and also the authors of this work, proposed a radical mechanism but without considering a chain sequence [10,26], while few authors excluded a radical mechanism [27]. Anyway, it is very probable that Mn species with different oxidation states exposed on the catalyst surface are involved in a redox cycle. For example, $Mn^{(n+1)+}$ species ($n = 2$ or 3) can be reduced to Mn^{n+} by H_2O_2 [25]:

$$H_2O_2 + Mn^{(n+1)+} \rightarrow H^+ + Mn^{n+} + HO_2^{\bullet} \quad (3)$$

Then the hydroperoxyl radical reacts with H_2O_2:

$$HO_2^{\bullet} + H_2O_2 \rightarrow O_2 + H_2O + HO^{\bullet} \quad (4)$$

The hydroxyl radical produced by reaction (4) re-oxidizes Mn^{n+} species:

$$Mn^{n+} + OH^{\bullet} \rightarrow Mn^{(n+1)+} + OH^- \quad (5)$$

The sequence of reactions (3)–(5), followed by the combination of H^+ with OH^-, is equivalent to the mechanism previously proposed for H_2O_2 decomposition in the liquid phase [10]. However, in this case, since the reactant is in the vapour phase, it is likely that radical species created on the catalyst surface initiate a chain reaction, as proposed by some authors [25]: this can be obtained by adding another reaction to the above scheme:

$$HO^{\bullet} + H_2O_2 \rightarrow H_2O + HO_2^{\bullet} \quad (6)$$

The reactions (4) and (6) form a chain sequence that is equivalent to the reaction of H_2O_2 decomposition. The chain could be terminated by reaction (5).

The autocatalytic effect can be explained considering the oxidizing action of O_2, that is the product of H_2O_2 decomposition: in fact O_2 can easily oxidize Mn^{n+} to $Mn^{(n+1)+}$, so increasing the rate of the Mn redox cycle and this obviously increases the global reaction rate. Moreover, the autocatalytic effect can be enhanced by a possible back diffusion of the product O_2, that is favoured by a low flow rate. This can explain the large increase of conversion observed with lowering of GHSV.

The activity of the support is not surprising, despite the hard reducibility of zirconia, because previous works [28,29] already reported the activity of zirconia for H_2O_2 decomposition. A likely intermediate of the reaction is the radical ion O_2^- that was detected by EPR [29]. Thus it is likely that the H_2O_2 decomposition occurs also on zirconia through a radical chain mechanism, such as that represented above (Eqs. (4) and (6)). The presence of the superoxide O_2^- can be explained by deprotonation of the $HO_2^{\bullet}$ radicals on the basic centres of zirconia [29]. The primary radicals that initiate the chain sequence are probably produced by the homolytic scission of the O—O bond of H_2O_2 [28]: this reaction has a high activation energy in the gas phase [30], but is strongly favoured on the ZrO_2 surface, where an activation energy of about 30–38 kJ mol^{-1} has been evaluated both theoretically and experimentally [28]. It is possible that a similar mechanism, not involving change of the oxidation state of the metal cations (Zr or Mn), contributes to H_2O_2 decomposition also on the Mn containing catalysts.

The autocatalytic effect, that is observed also with the pure support, can be due to the product O_2 according to the following reactions:

$$H_2O_2 \leftrightarrows H^+ + HO_2^- \quad (7)$$

$$O_2 + HO_2^- \rightarrow O_2^- + HO_2^{\bullet} \quad (8)$$

Reaction (8) can be favoured by adsorption of O_2 on anion vacancies that are present on the surface of zirconia [9,31]. Reaction (8) produces two radical species that obviously promote the H_2O_2 decomposition.

A comparison between the studied catalysts shows that the performances obtained with the catalyst prepared by sol gel coating are comparable or better than those obtained with catalysts prepared by precipitation or impregnation: in fact, at GHSV = 2.76 s^{-1}, the higher conversion of H_2O_2 was obtained on the SG catalyst, while at GHSV = 2.00 s^{-1}, the H_2O_2 conversions on SG, PR and IM were not very different. As discussed above, at lower GHSV the conversion is increased by an autocatalytic effect probably favoured by a retro-diffusion of the product O_2. This effect appears stronger for the PR catalyst, while for IM, and especially for SG, it is more limited. The reason of this different behaviour is not clear, but it can be supposed that the effect of autocatalysis depends on the rate of reaction between Mn ions and O_2: probably this reaction is slower with the SG catalyst due to the strong interaction between Mn ions and zirconia, but this hypothesis needs to be supported by other data. It is expected that the autocatalytic effect will be less important in real propulsive applications, in which much higher feed flow rates will be used. Therefore the results obtained at higher GHSV are probably more significant for a comparison between different catalysts, being less influenced by the action of the product O_2. Under these conditions, the higher activity of SG can be related to the presence of Mn species with a higher reducibility, as suggested by TPR data. Fig. 4 shows that the reduction of SG begins at lower temperature compared with the other catalysts: this indicates the presence of more reducible Mn species that can favour reaction (3), the first step of the proposed mechanism. Moreover it must be noted that the high activity of the catalyst SG was obtained despite the lower Mn content of this catalyst. This can be probably explained by a higher Mn dispersion that leads to a higher amount of Mn exposed on the surface and active for the reaction.

4. Conclusions

This work shows that the new test apparatus allows an easy and simple evaluation of the catalytic activity for H_2O_2 decomposition in the vapour phase, under flow conditions. The apparatus was

employed to compare the activity of new monolithic catalysts prepared by the techniques of sol–gel dip coating, precipitation and vacuum impregnation. The results indicate that the performance for H_2O_2 decomposition of the catalyst prepared by sol–gel coating is comparable or better than that obtained with catalysts prepared by precipitation or impregnation. The sol–gel coating method gives the advantage of a higher Mn dispersion: on the other hand, due to the strong interaction with the dispersing zirconia matrix, a large fraction of Mn is maintained in a stable oxidation state that is probably less active for H_2O_2 decomposition.

References

[1] R. Brahmi, Y. Batonneau, C. Kappenstein, P. Miotti, M. Tajmar, C. Scharlemann, M. Lang, Studies in Surface Science and Catalysis 162 (2006) 649–656.
[2] A. Pasini, L. Torre, L. Romeo, A. Cervone, L. d'Agostino, Journal of Propulsion and Power 24 (2008) 507–515.
[3] A. Russo Sorge, M. Turco, G. Pilone, G. Bagnasco, Journal of Propulsion and Power 20 (2004) 1069–1075.
[4] C. Kappenstein, L. Pirault-Roy, M. Guérin, T. Wahdan, A.A. Ali, F. Al-Sagheer, M.I. Zaki, Applied Catalysis A: General 234 (2002) 145–153.
[5] S.H. Do, B. Batchelor, H.K. Lee, S.H. Kong, Chemosphere 75 (2009) 8–12.
[6] L. Pirault-Roy, C. Kappenstein, M. Guérin, R. Eloirdi, Journal of Propulsion and Power 16 (2002) 1235–1241.
[7] M.A. Hasan, M. Zaki, L. Pasupulety, K. Kumari, Applied Catalysis A: General 181 (1999) 171–179.
[8] J.J. Rusek, Journal of Propulsion and Power 12 (1996) 574–579.
[9] M. Turco, G. Bagnasco, A. Russo Sorge, Chemical Engineering Transactions 6 (2005) 39–44.
[10] E. Fanelli, M. Turco, A. Russo, G. Bagnasco, S. Marchese, P. Pernice, A. Aronne, Journal of Sol–Gel Science and Technology 60 (2011) 426–436.
[11] C.N. Satterfield, R.S.C. Yeung, Industrial and Engineering Chemistry Fundamentals 2 (1963) 257–264.
[12] D. Amariei, R. Amrousse, Y. Batonneau, R. Brahmi, C. Kappenstein, B. Cartoixa, Studies in Surface Science and Catalysis 175 (2010) 35–42.
[13] R. Amrousse, R. Brahmi, Y. Batonneau, C. Kappenstein, M. Théron, P. Bravais, Studies in Surface Science and Catalysis 175 (2010) 755–758.
[14] N.D.S. Mohallem, M.M. Viana, R.A. Silva, Automotive catalysts: performance, characterization and development, in: M. Chiaberge (Ed.), New Trends and Developments in Automotive Industry, InTech, 2011, pp. 347–364 (Chapter 19).
[15] X.M. Liu, S.Y. Fu, C.J. Huang, Powder Technology 154 (2005) 120–124.
[16] A.K.H Nohman, H.M. Ismail, G.A.M. Hussein, Journal of Analytical and Applied Pyrolysis 34 (1995) 265–278.
[17] M. Turco, G. Bagnasco, C. Cammarano, L. Micoli, M. Lenarda, E. Moretti, L. Storaro, A. Talon, Applied Catalysis B: Environmental 102 (2011) 387–394.
[18] F. Rouquerol, J. Rouquerol, K. Sing, Adsorption by Powders and Porous Solids, Academic Press, London, 1999.
[19] S. Geller, Acta Crystallographica 27 (1971) 821–828.
[20] S. Fritsch, A. Navrotsky, Journal of the American Ceramic Society 79 (1996) 1761–1768.
[21] T.J.W. De Bruijn, W.A. De Jong, P.J. Van Den Berg, Thermochimica Acta 45 (1981) 265–278.
[22] S. Chytil, A. Linda, E. Vanhaeckeb, E.A. Blekkanb, Energy Procedia 26 (2012) 98–106.
[23] L. Gao, L. Zhou, C. Li, J. Feng, Y. Lu, Journal of Materials Science 48 (2013) 974–977.
[24] P. Kirchner, J. Oberlaender, P. Friedrich, J. Berger, H.P. Suso, A. Kupyna, M. Keusgen, M.J. Schoening, Physical Status Solidi A 208 (2011) 1235–1240.
[25] A.K.H. Nohman, M.I. Zaki, European Space Agency [Special Publication] SP (2006), SP-635 (3rd International Conference on Green Propellant for Space Propulsion and 9th International Hydrogen Peroxide Propulsion Conference, 2006), ESA Publications Division, 2006.
[26] I.A. Salem, R.I. Elhag, K.M.S. Khalil, Transition Metal Chemistry 25 (2000) 260–264.
[27] Y.N. Lee, R.M. Lago, J.L.G. Fierro, J. González, Applied Catalysis A: General 215 (2001) 245–256.
[28] C.M. Lousada, A.J. Johansson, T. Brinck, M. Jonsson, Journal of Physical Chemistry 116 (2012) 9533–9543.
[29] E. Giamello, P. Rumori, F. Geobaldo, B. Fubini, M.C. Paganini, Applied Magnetic Resonance 10 (1996) 173–192.
[30] J. Troe, Combustion and Flame 158 (2011) 594–601.
[31] Y. Li, D. He, Q. Zhu, X. Zhang, B. Xu, Journal of Catalysis 221 (2004) 584–593.